in combination with periodic reservoir reloading from a cold atom source (such as a MOT), could be used to maintain arrays indefinitely.

Atom-by-atom assembly of defect-free arrays forms a scalable platform with unique possibilities. It combines features that are typically associated with ion-trapping experiments, such as single-qubit addressability (32, 33) and fast cycling times, with the flexible optical trapping of neutral atoms in a scalable fashion. Furthermore, in contrast to solid-state platforms, such atomic arrays are highly homogeneous (31) and mostly decoupled from their environment. The homogeneity of our array should also allow for cooling of the atomic motion via simultaneous sideband cooling in all tweezers at once (34, 35).

These features provide an excellent starting point for multiqubit experiments, for studies of quantum many-body effects, and for exploring future applications. The required interactions between the atoms can be engineered using several approaches. Even without sideband cooling, exciting the atoms into high-lying Rydberg states would introduce strong dipole interactions that can be used for fast entangling gates (24, 25, 27). The parallelism afforded by our flexible atom rearrangement enables efficient diagnostics of such Rydberg-mediated entanglement. These interactions may also enable approaches to quantum simulations that involve both coherent coupling and engineered dissipation (26, 27), as well as large-scale entangled quantum states for applications in precision measurements (36).

An alternative approach to engineering interactions involves the integration of atom arrays with nanophotonic platforms as demonstrated previously (28, 29). These enable photon-mediated interactions that can be employed to couple the atoms within a local multiqubit register or for efficient communication between the registers using a modular quantum network architecture (3).

Finally, our platform could enable new bottom-up approaches to studying quantum many-body physics in Hubbard models (15, 16, 30), where atomic Mott insulators with fixed atom number and complex spin patterns could be directly assembled. This requires atom temperatures close to the ground state, coherent tunneling between the traps, and sizable on-site interactions. With side-band cooling, ground-state fractions in excess of 90% have already been demonstrated (34, 35) and can likely be improved via additional optical trapping along the longitudinal tweezer axes, which would also increase on-site interaction strengths. Coherent tunneling of Rb atoms between similarly sized tweezers has been observed before by reducing the tweezer distance (15, 16). The parametric heating, currently limiting the minimal distance between our traps, could be reduced by working with shallower traps, as needed for tunneling, and by employing fewer traps to increase the frequency separation between neighboring traps. Eventually, this approach could be applied to create ultracold quantum matter composed of exotic atomic species or complex molecules (37, 38) that are difficult to cool evaporatively.

## REFERENCES AND NOTES

1. S. Haroche, *Ann. Phys.* **525**, 753–776 (2013).
2. D. J. Wineland, *Rev. Mod. Phys.* **85**, 1103–1114 (2013).
3. C. Monroe, J. Kim, *Science* **339**, 1164–1169 (2013).
4. M. H. Devoret, R. J. Schoelkopf, *Science* **339**, 1169–1174 (2013).
5. W. S. Bakr *et al.*, *Science* **329**, 547–550 (2010).
6. J. F. Sherson *et al.*, *Nature* **467**, 68–72 (2010).
7. C. Weitenberg *et al.*, *Nature* **471**, 319–324 (2011).
8. D. S. Weiss *et al.*, *Phys. Rev. A* **70**, 040302 (2004).
9. J. Vala *et al.*, *Phys. Rev. A* **71**, 032324 (2005).
10. N. Schlosser, G. Reymond, I. Protsenko, P. Grangier, *Nature* **411**, 1024–1027 (2001).
11. M. Weber, J. Volz, K. Saucke, C. Kurtsiefer, H. Weinfurter, *Phys. Rev. A* **73**, 043406 (2006).
12. K. D. Nelson, X. Li, D. S. Weiss, *Nat. Phys.* **3**, 556–560 (2007).
13. M. J. Piotrowicz *et al.*, *Phys. Rev. A* **88**, 013420 (2013).
14. F. Nogrette *et al.*, *Phys. Rev. X* **4**, 021034 (2014).
15. A. M. Kaufman *et al.*, *Science* **345**, 306–309 (2014).
16. A. M. Kaufman *et al.*, *Nature* **527**, 208–211 (2015).
17. Y. Miroshnychenko *et al.*, *Nature* **442**, 151 (2006).
18. J. Beugnon *et al.*, *Nat. Phys.* **3**, 696–699 (2007).
19. M. Schlosser *et al.*, *New J. Phys.* **14**, 123034 (2012).
20. H. Kim, *et al.*, *Nat. Commun.* **7**, 13317 (2016).
21. T. Grünzweig, A. Hilliard, M. McGovern, M. F. Andersen, *Nat. Phys.* **6**, 951–954 (2010).
22. B. J. Lester, N. Luick, A. M. Kaufman, C. M. Reynolds, C. A. Regal, *Phys. Rev. Lett.* **115**, 073003 (2015).
23. Y. H. Fung, M. F. Andersen, *New J. Phys.* **17**, 073011 (2015).
24. D. Jaksch *et al.*, *Phys. Rev. Lett.* **85**, 2208–2211 (2000).
25. M. Saffman, T. G. Walker, K. Mølmer, *Rev. Mod. Phys.* **82**, 2313–2363 (2010).
26. H. Weimer, M. Müller, I. Lesanovsky, P. Zoller, H. P. Büchler, *Nat. Phys.* **6**, 382–388 (2010).
27. A. Browaeys, D. Barredo, T. Lahaye, *J. Phys. B* **49**, 152001 (2016).
28. J. D. Thompson *et al.*, *Science* **340**, 1202–1205 (2013).
29. A. Goban *et al.*, *Nat. Commun.* **5**, 3808 (2014).
30. S. Murmann *et al.*, *Phys. Rev. Lett.* **115**, 215301 (2015).
31. See supplementary materials on *Science* Online.
32. T. Xia *et al.*, *Phys. Rev. Lett.* **114**, 100503 (2015).
33. Y. Wang, X. Zhang, T. A. Corcovilos, A. Kumar, D. S. Weiss, *Phys. Rev. Lett.* **115**, 043003 (2015).
34. A. M. Kaufman, B. J. Lester, C. A. Regal, *Phys. Rev. X* **2**, 041014 (2012).
35. J. D. Thompson, T. G. Tiecke, A. S. Zibrov, V. Vuletić, M. D. Lukin, *Phys. Rev. Lett.* **110**, 133001 (2013).
36. P. Kómár *et al.*, *Phys. Rev. Lett.* **117**, 060506 (2016).
37. J. F. Barry, D. J. McCarron, E. B. Norrgard, M. H. Steinecker, D. DeMille, *Nature* **512**, 286–289 (2014).
38. N. R. Hutzler, L. R. Liu, Y. Yu, K.-K. Ni, https://arxiv.org/abs/1605.09422 (2016).
39. D. Barredo, S. de Léséleuc, V. Lienhard, T. Lahaye, A. Browaeys, *Science* **354**, 1021–1023 (2016).

---

## GEOPHYSICS

# Mega-earthquakes rupture flat megathrusts

Quentin Bletery,[1]* Amanda M. Thomas,[1] Alan W. Rempel,[1] Leif Karlstrom,[1] Anthony Sladen,[2] Louis De Barros[2]

The 2004 Sumatra-Andaman and 2011 Tohoku-Oki earthquakes highlighted gaps in our understanding of mega-earthquake rupture processes and the factors controlling their global distribution: A fast convergence rate and young buoyant lithosphere are not required to produce mega-earthquakes. We calculated the curvature along the major subduction zones of the world, showing that mega-earthquakes preferentially rupture flat (low-curvature) interfaces. A simplified analytic model demonstrates that heterogeneity in shear strength increases with curvature. Shear strength on flat megathrusts is more homogeneous, and hence more likely to be exceeded simultaneously over large areas, than on highly curved faults.

Past mega-earthquakes, such as the magnitude (M) 9.6 Chile earthquake in 1960 and the M 9.3 Alaska earthquake in 1964, occurred in areas where the subducting lithosphere was relatively young (and buoyant) and the plate convergence rate was relatively high (1). These observations led some authors to hypothesize that maximum earthquake size is controlled by these two geological parameters (2, 3). The development of space-based geodesy enabled refined measurements of plate motion that challenged the role of convergence rate (4–6). Additionally, the moment magnitude ($M_w$) 9.0 Tohoku-Oki earthquake (7) ruptured lithosphere that is over 120 million years old (8), ruling out lithospheric age as the dominant control. Weak correlations appear in recent data sets among a variety of parameters, including forearc structure (9, 10); age, density, and buoyancy of the slab (6); upper plate motion (11); upper plate strain (12); long-term trench migration (11); trench sediment thickness (12); and width of the seismogenic

[1]Department of Earth Sciences, University of Oregon, 1272 University of Oregon, Eugene, OR 97403, USA. [2]Université Côte d'Azur, CNRS, OCA, IRD, Géoazur, 250 rue Albert Einstein, Sophia Antipolis, 06560 Valbonne, France.
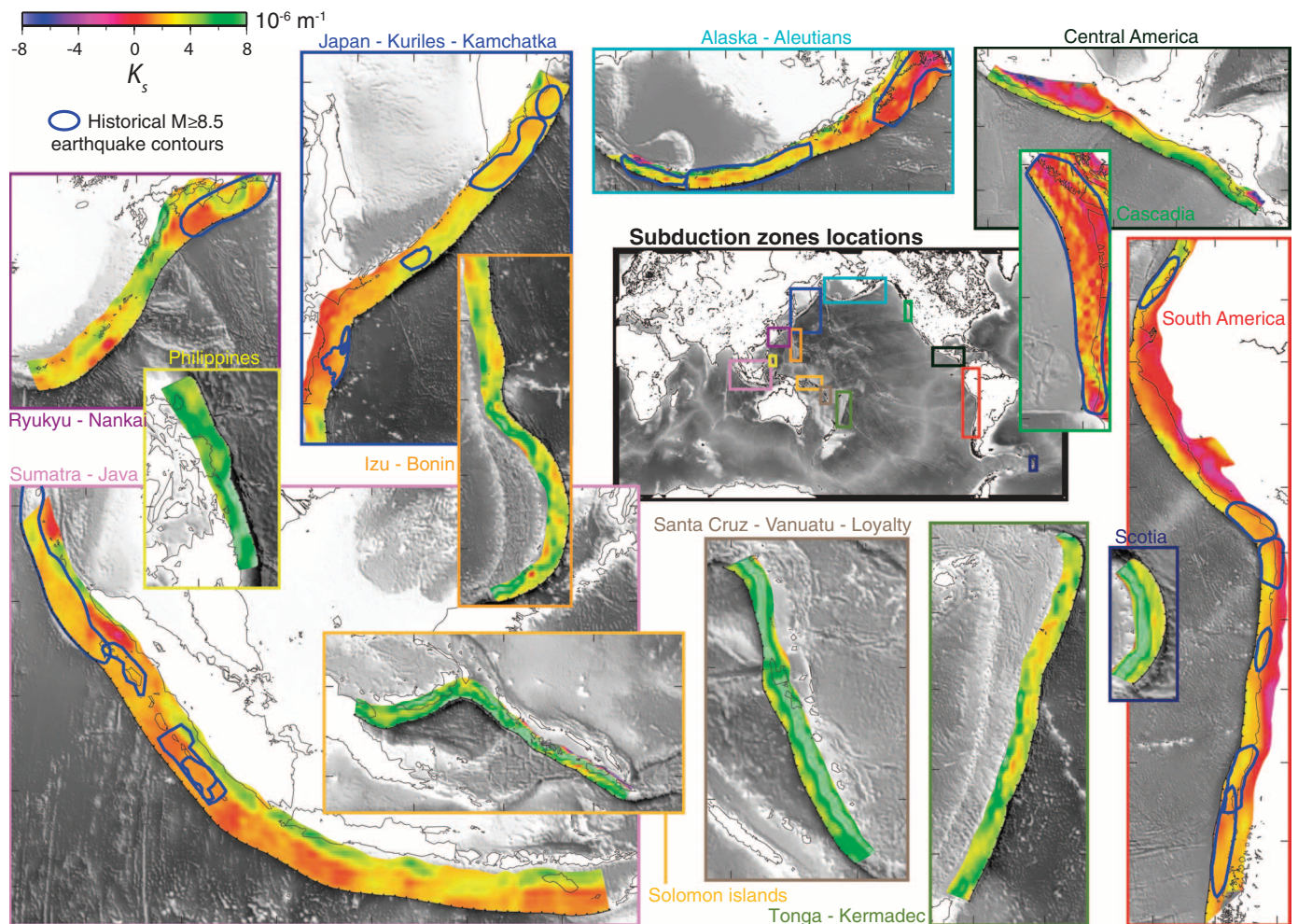*Corresponding author. Email: qbletery@uoregon.edu

**Fig. 1. Variations in megathrust curvature and distribution of historical mega-earthquakes.** Along-dip curvature $K_s = d\theta/ds$ on the megathrust is shown for the 13 main subduction zones of the world, overlaid with the estimated slip contours of known historical mega-earthquakes ($M \geq 8.5$) (see table S1 for a list of events). Tick marks in each panel are spaced at 5° increments.

zone (11, 13, 14). However, aside from dip angle and seismogenic width [coefficient of correlation $r = 0.61$ (14)], none of these parameters correlate strongly ($|r| < 0.5$) with the maximum earthquake magnitude recorded in the different zones (11). Stronger correlations are found with fault properties such as thrust interface dip angle (11) and apparent friction derived from heat flow measurements (15).

Today, forecasts of potential large earthquakes focus mainly on imaging the slip deficit with respect to the relative plate motion, because such deficits are thought to result in stress loading that is ultimately released in earthquakes [e.g., (16)]. We followed a complementary approach by analyzing large-scale geometrical features of subduction faults and assessing their possible influence on the physical conditions favoring large earthquake ruptures. Seismic moment $M_0 \propto \Delta\sigma S^{3/2}$ (17) depends mainly on the surface area $S$ over which an earthquake ruptures, because the stress drop $\Delta\sigma$ (the difference in stress before and after an earthquake) is roughly constant among earthquakes over a large range of magnitudes (18). Here we demonstrate that slab interface curvature

exerts a leading-order control on the spatial extent of potential ruptures in subduction zones and hence on the magnitude of the largest earthquakes.

Data sets from active- and passive-source seismology have been combined to constrain the slab1.0 model for the geometry of the world's major subduction zones (14) [details and limitations of the slab1.0 model are discussed in the supplementary materials (19)]. We computed maps of the along-dip interface curvature $K_s = d\theta/ds$, hereafter referred to as curvature [where $\theta$ is the dip angle and $s$ is the tangent to the interface pointing in the down-dip direction (19)], using the slab1.0 model (14, 20) (Fig. 1). Because $K_s$ is almost always positive (Fig. 1), we hereafter interchangeably refer to low-$K_s$ fault regions as flat, low-curvature, or planar. Similarly, we computed the along-strike gradient of the dip angle $K_t = d\theta/dt$ (fig. S1). Comparison with a catalog of historical events (19) reveals a tendency for mega-earthquakes to occur on relatively flat (low-$K_s$) megathrusts (Fig. 1). The curvature is particularly small in the Japan-Kuriles-Kamchatka, Alaska-Aleutians, Sumatra-Java, South America, and Cascadia subduction zones, which are known

to produce $M \geq 9.0$ earthquakes. Subduction zones with large curvatures, such as the Philippines, Solomon Islands, Izu-Bonin, Santa Cruz–Vanuatu-Loyalty, and Tonga-Kermadec zones, lack historic mega-earthquakes. At a smaller scale, we also observe that the down-dip limit of mega-earthquakes offshore of Sumatra—and to a lesser extent, in the Aleutians, Alaska, Nankai, and Kamchatka—coincides with an abrupt change in the slope, suggesting that the conditions required to generate large earthquakes are directly related to the local curvature along the megathrust interface.

To further explore the role of subduction geometry, we calculated the average dip angle $\bar{\theta}$ (Fig. 2A), the average curvature $\overline{K_s}$ (Fig. 2B), and the average along-strike gradient of dip angle $\overline{|K_t|}$ (fig. S2) from the trench to 60 km depth, and we compared these values with the magnitude of the largest megathrust earthquake $M_{max}$ recorded in each subduction zone. We found that $M_{max}$ anticorrelates ($r = -0.72$) with $\bar{\theta}$ (Fig. 2A) and anticorrelates even more strongly ($r = -0.80$) with $\overline{K_s}$ (Fig. 2B). The anticorrelation with $\overline{|K_t|}$ is weaker ($r = -0.64$) but still significant (fig.

**A** $\overline{\theta} = f(M_{max})$ ?
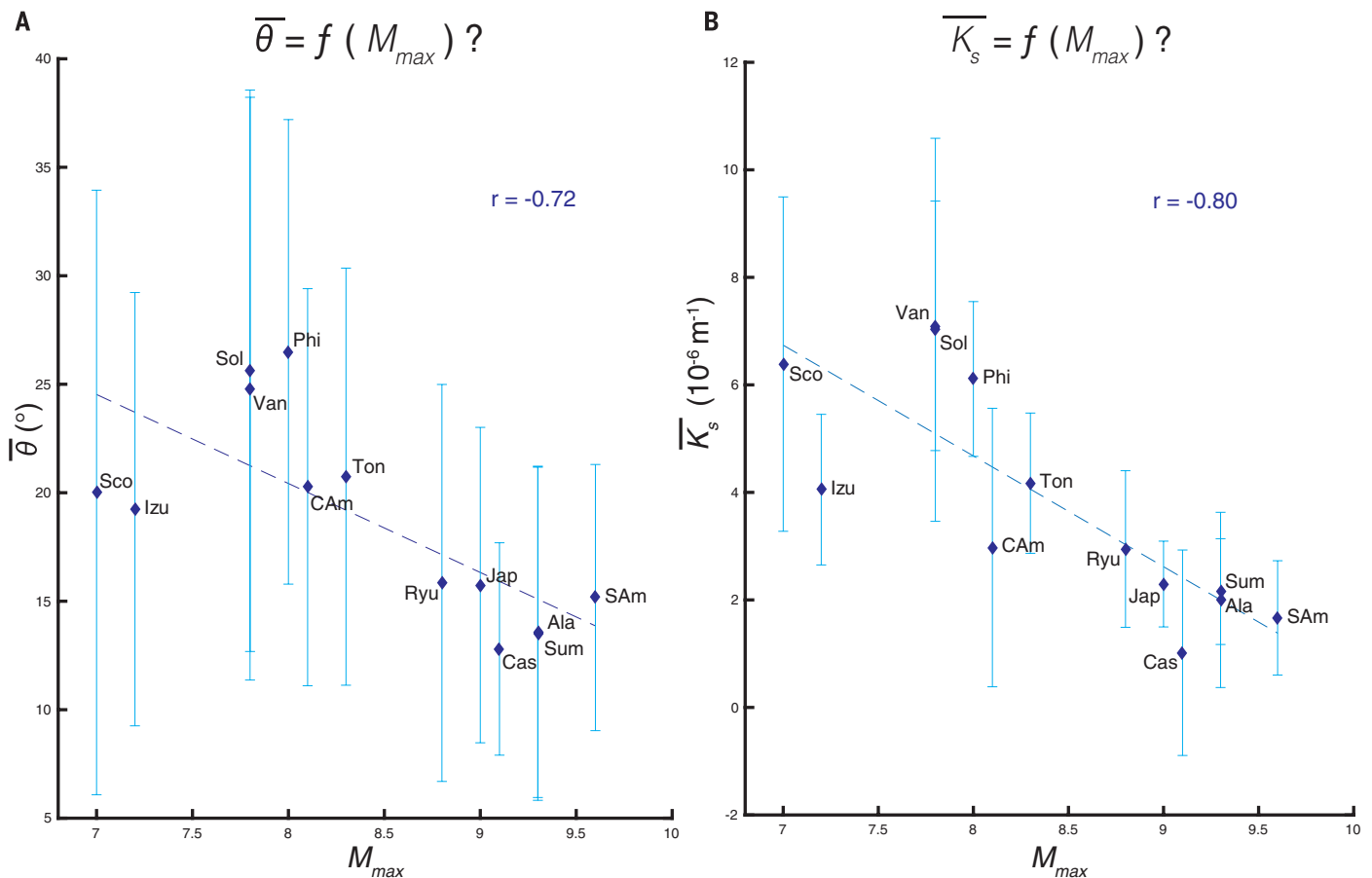
**B** $\overline{K_s} = f(M_{max})$ ?

**Fig. 2. Correlation of average dip angle and curvature with maximum earthquake magnitude.** (**A**) Average dip angle $\overline{\theta}$ of the 13 main subduction zones of the world as a function of the maximum event magnitude $M_{max}$ recorded on the megathrust (see table S2 for a list of events). The coefficient of correlation $r$ is −0.72. (**B**) Same as (A), but for the average along-dip curvature $\overline{K_s}$ ($r$ = −0.80). Light blue bars show the standard deviation for the distribution of $\overline{\theta}$ (A) and $\overline{K_s}$ (B) in each subduction zone. These bars should not be considered as error bars because we are reasoning with averages; they rather indicate how $\theta$ and $K_s$ are distributed along the different subduction zones. Blue dashed lines are the linear regressions. Ala, Alaska-Aleutians; CAm, Central America; Cas, Cascadia; Izu, Izu-Bonin; Jap, Japan-Kuriles-Kamchatka; Phi, Philippines; Ryu, Ryukyu-Nankai; SAm, South America; Sco, Scotia arc; Sol, Solomon Islands; Sum, Sumatra-Java; Ton, Tonga-Kermadec; Van, Santa Cruz–Vanuatu-Loyalty.

S2). We suggest, on the basis of our observations, that planar slab interfaces are prone to hosting larger earthquakes. Multiple factors, including the subducting (21) or overriding (22) plate thickness and viscosity contrast (23), have been invoked as controls on subduction curvature; these studies (21–23) provide a useful introduction to this field of research.

The average curvature within mega-earthquake slip contours is consistent with the linear regression in Fig. 2B, with observed values always smaller than $3.76 \times 10^{-6}$ m$^{-1}$ (fig. S5B). Given the distribution of $K_s$ across the different megathrusts of the world, the likelihood that all known mega-earthquakes occurred by chance on $K_s \leq 3.76 \times 10^{-6}$ m$^{-1}$ areas is 0.8% (19), allowing us to affirm with >99% confidence that earthquake magnitude is related to megathrust curvature. The distribution of the average dip angle within mega-rupture contours is much broader (fig. S5A), confirming the stronger relationship of earthquake size with curvature than with dip angle (19). Nevertheless, known mega-earthquakes do not exhibit a strong tendency to rupture the lower-curvature portions of their host subduction zones (19). This suggests that over the long term, mega-earthquakes might rupture any portion of a low-curvature subduction thrust, such as those of the Cascadia, South America, Alaska-Aleutians, Sumatra-Java, Japan-Kuriles-Kamchatka, Ryukyu-Nankai, and Central America subduction zones. Large earthquakes are preferentially hosted by megathrusts with low dip angles in part as a consequence of larger down-dip seismogenic extents making ruptures possible over wider fault areas (11, 13, 14). However, the stronger relationship of earthquake size with curvature than with dip angle noted above (Fig. 2B) warrants a more thorough description of fault loading.

The present understanding of seismic ruptures can be framed in terms of the asperity model: Earthquakes are caused by the sudden failure of locked macroscopic asperities that accumulate stress during interseismic periods (24). In this context, the extent of an earthquake has a leading-order dependence on the size of the rupturing asperity and the neighboring region that is pushed to failure by coseismic stress change.

Recent efforts aimed at characterizing the nature of asperities and their immediate surroundings have mostly focused on potential variations in friction along faults [e.g, (25–28)]. The capacity of a fault segment to accumulate stress is bounded by the Coulomb failure criterion

$$|\tau^c| = \mu(\sigma_n^c - p) \qquad (1)$$

where $\tau^c$ is the critical shear stress required to initiate a rupture (hereafter referred to as shear strength), $\mu$ is the coefficient of friction, $p$ is the pore pressure, $\sigma_n^c$ is the normal stress when the rupture initiates, and cohesion is neglected. The Coulomb failure criterion is met when the accumulated shear stress reaches the frictional shear strength and an earthquake initiates. From Eq. 1, one can define an asperity as a fault area characterized by a particularly high friction coefficient $\mu$. Alternatively, one can also explain the time-dependent behavior of asperities by appealing to variations in pore pressure $p$ that accompany fluid migration [e.g., (29)]. We explore here a different hypothesis, which is that the locations of

asperities can be determined by analyzing variations in normal stress $\sigma_n$ that are governed by large-scale geometrical characteristics of megathrust interfaces. Assuming constant friction $\mu$ and hydrostatic pore pressure $p = \rho_w g h$ (with $\rho_w$ being the water density, $g$ the acceleration of gravity, and $h$ the local interface depth), we illustrate the effect of variations in normal stress $\sigma_n$ on variations in shear strength [this method is reminiscent of the consideration of normal force in (16) but invokes different causative factors, i.e., curvature instead of plate tectonic forces].

We considered a simple two-dimensional (2D) fault model: a fault interface subjected to the pressure of the upper plate mass and an unknown horizontal tectonic stress. We also treated the convergence direction as aligned with the horizontal projection of the local along-dip direction (i.e., pure dip-slip convergence). This latter simplification is justified by the dominantly dip-slip mechanisms of most megathrust earthquakes [e.g., figures 14, 15, and 16 of (30)]. Even though subduction zones present, to varying degrees, oblique convergences, this obliquity is usually accommodated for the most part by large strike-slip faults in the back arc. One notable exception is the Solomon Islands subduction zone, which presents a very strong oblique convergence and hosts megathrust earthquakes that typically exhibit large strike-slip components. Our idealized description of the convergence direction allows us to treat the 3D problem with a 2D model (fig. S6). Within this framework, the shear strength—defined as the critical shear stress required to initiate slip at a given location—can be expressed as a function of the crustal density $\rho$, the friction $\mu$, the depth $h$, the dip angle $\theta$, and the angle $\psi$ between the maximum principal component of stress and the horizontal

$$\tau^c = \frac{g h \mu (\rho - \rho_w)(\sin 2\theta + \tan 2\psi \cos 2\theta)}{\sin 2\theta - \mu(1 - \cos 2\theta) + \tan 2\psi(\cos 2\theta - \mu \sin 2\theta)} \quad (2)$$

$\tau^c$ increases with $\theta$ ($\partial \tau^c / \partial \theta \geq 0$) (19) meaning that large dip angles imply greater shear strength. If the dominant control of earthquake magnitude were the amplitude of shear strength, we might expect a positive correlation between $M_{max}$ and $\theta$. The negative correlation that we observe (Fig. 2A) points to other factors.

Because the magnitude of an earthquake is primarily controlled by the area of rupture, homogeneous distributions of shear strength over large fault areas may favor the occurrence of mega-earthquakes. In this framework, the shear-strength gradient $d\tau^c/ds$ is a critical parameter. Treating $\mu$, $\rho$, $\rho_w$, and $g$ as constants, spatial variations of $\tau^c$ obtained by differentiation of Eq. 2 satisfy

$$\frac{d\tau^c}{ds} = g\mu(\rho - \rho_w)\Big(A_\mu(\theta, \psi)\sin\theta +$$

$$B_\mu(\theta, \psi)hK_s + C_\mu(\theta, \psi)h\frac{d\psi}{ds}\Big) \quad (3)$$

where $\rho > \rho_w$ and the functions $A_\mu(\theta, \psi)$, $B_\mu(\theta, \psi)$, and $C_\mu(\theta, \psi)$ are positive for $\mu = 0.6$ and values of $\theta$ and $\psi$ typically encountered in subduction zones (19). Therefore, $|d\tau^c/ds|$ increases with $K_s$ [a similar argument can be made to show that $|d\tau/dt|$ increases, on average, with $|K_t|$ (19)]. Shear-strength heterogeneity increases with curvature: The flatter the megathrust interface (lower $K_s$), the more homogeneous the shear-strength distribution. Stress accumulation along faults is complex, and heterogeneities in driving stress can result from the effect of stress concentrations inherited from past events or changes in coupling associated with variations in the friction coefficient or pore fluid pressure. However, dynamic stress perturbations induced by earthquake propagation are more likely to overstep the resistance to failure over broad areas if shear strength is homogeneously distributed along a large fault surface. In contrast, barriers to earthquake propagation are more likely for heterogeneous shear-strength distributions, because the dynamic stress perturbations required to reach local values of shear strength will tend to be larger in some regions. The idea that geometrical heterogeneity may limit earthquake propagation has been previously invoked (15, 31) and is consistent with the observation that many large earthquake ruptures terminate near subducting seamounts or other structural heterogeneities (31, 32).

During an earthquake, fault slip will propagate as long as the dynamic stress perturbation induced by the earlier phase of the rupture, $\delta\tau$, is larger than the difference between shear strength and shear stress in the surrounding area, $\Delta\tau$. Hence, one way to generate mega-earthquakes is to initiate a large dynamic stress perturbation by the failure of a strongly locked asperity so that $\delta\tau > \Delta\tau$ over a large surrounding fault area. In this scenario, mega-earthquakes are characterized by the rupture of one or several asperities where shear strength is particularly high. Our finding that large earthquakes rupture flat megathrusts suggests that another way to generate mega-earthquakes is if $\Delta\tau$ is small in a large area surrounding rupture nucleation, and thus even relatively small dynamic stress perturbations $\delta\tau$ can continue to propagate rupture. The 2004 Sumatra-Andaman earthquake, a unilaterally propagating 1600-km-long rupture without evidence of a localized high stress drop (33), exemplifies this second scenario, because it is unlikely that the energy released during the early phases of rupture could have initiated slip on fault portions as far as 1600 km away if the entire ruptured area was not already close to failure. In this situation, mega-earthquakes are not characterized by the rupture of asperities in regions where strength is much greater than in the surrounding area but, on the contrary, by the absence of strong variations in strength. The limiting case of homogeneous null shear strength results in constant creep and the absence of earthquakes of any magnitude. Hence, although the amplitude of $\tau^c$ is an important parameter, the observation that mega-earthquakes preferentially occur on flat subduction zones (Fig. 2) seems to indicate that the homogeneity of the shear-strength distribution is among the most critical factors in enabling the generation of mega-earthquakes.

It has recently been proposed that any subduction zone may produce a $M \geq 9$ earthquake (34). Our results suggest that earthquake size is limited by curvature and, if our interpretation is correct, mega-earthquakes might be physically incapable of rupturing highly curved subduction zones with large shear-strength gradients, such as the Philippines, the Solomon Islands, Scotia arc, and Santa Cruz–Vanuatu-Loyalty; heterogeneous shear strength creates natural barriers that stop earthquake propagation. It is possible that heterogeneous shear stress could build to match a heterogeneous shear-strength distribution and allow rare large events, but such scenarios are expected to be less likely, and therefore more infrequent, than on megathrusts with more homogeneous shear strength. As indicated by Fig. 2B, some subduction zones, such as Izu-Bonin or Central America, may yet host earthquakes larger than previously recorded. Cascadia is noteworthy because the last mega-earthquake that it hosted is thought to have ruptured the entire subduction fault and therefore reached the maximum possible magnitude for this subduction zone (35). At a smaller scale, some areas, such as Peru, Java, or the large low-to-negative $K_s$ fault region in Central America (Fig. 1), which includes the Guerrero gap but extends much farther, show favorable features for a possible very large rupture—implying in the Guerrero case the potential for an even larger earthquake than that inferred from the extent of the gap. Moreover, large flat portions of subduction faults may sometimes rupture as one mega-earthquake and sometimes as several smaller earthquakes. Such behavior is documented, for instance, in Nankai (36), where two nearby asperities sometimes break as two separate consecutive earthquakes (as in 1854 and 1944–1946) and sometimes as one larger earthquake (1707; blue contour in the Ryukyu-Nankai box). This suggests that high-curvature regions of generally flat subduction zones may act as barriers to rupture most of the time and still sometimes be overcome by coseismic stress changes. Planar fault areas may thus host moderate-sized earthquakes for a long time and still have the potential to generate mega-earthquakes in the future.

It is possible that frictional properties and geometry are related. Such mechanical relationships are well described in accretionary wedges (37) and are certainly expected, though more difficult to constrain, along the deeper portions of megathrusts. Slab curvature has also been proposed to promote higher permeability (38–41) and thus to have an impact on the pore fluid pressure as well. Nevertheless, we have shown that spatial variations in friction and pore fluid pressure are not required to explain the gross distribution of mega-earthquakes. The observation that mega-earthquakes preferentially rupture flat megathrusts (Figs. 1 and 2B) is consistent with the inference that shear strength tends to be more homogeneously distributed along such subduction interfaces (Eq. 3), facilitating synchronized

failure over large areas. This implies that the critical feature at play in the generation of mega-earthquakes is not the amplitude of shear strength but its spatial variations. Thus, the absence of asperities on large faults may counterintuitively be a source of higher hazard. Though our study focused on subduction earthquakes, flatness may favor large earthquakes on long strike-slip faults as well.

## REFERENCES AND NOTES

1. H. Kanamori, *Philos. Trans. R. Soc. A* **364**, 1927–1945 (2006).
2. L. Ruff, H. Kanamori, *Phys. Earth Planet. Inter.* **23**, 240–252 (1980).
3. L. Ruff, H. Kanamori, *Tectonophysics* **99**, 99–117 (1983).
4. R. McCaffrey, *Geophys. Res. Lett.* **21**, 2327–2330 (1994).
5. S. Stein, E. A. Okal, *Bull. Seismol. Soc. Am.* **97**, S279–S295 (2007).
6. T. Nishikawa, S. Ide, *Nat. Geosci.* **7**, 904–908 (2014).
7. Q. Bletery *et al.*, *J. Geophys. Res. Solid Earth* **119**, 7636–7653 (2014).
8. R. D. Müller, M. Sdrolias, C. Gaina, W. R. Roest, *Geochem. Geophys. Geosyst.* **9**, Q04006 (2008).
9. T.-R. A. Song, M. Simons, *Science* **301**, 630–633 (2003).
10. R. E. Wells, R. J. Blakely, Y. Sugiyama, D. W. Scholl, P. A. Dinterman, *J. Geophys. Res. Solid Earth* **108**, 2507 (2003).
11. W. Schellart, N. Rawlinson, *Phys. Earth Planet. Inter.* **225**, 41–67 (2013).
12. A. Heuret, C. Conrad, F. Funiciello, S. Lallemand, L. Sandri, *Geophys. Res. Lett.* **39**, L05304 (2012).
13. J. F. Pacheco, L. R. Sykes, *Bull. Seismol. Soc. Am.* **82**, 1306 (1992).
14. G. P. Hayes, D. J. Wald, R. L. Johnson, *J. Geophys. Res. Solid Earth* **117**, B01302 (2012).
15. X. Gao, K. Wang, *Science* **345**, 1038–1041 (2014).
16. C. H. Scholz, J. Campos, *J. Geophys. Res. Solid Earth* **117**, B05310 (2012).
17. R. Madariaga, *J. Geophys. Res.* **84**, 2243 (1979).
18. H. Kanamori, D. L. Anderson, *J. Geophys. Res.* **80**, 1075–1078 (1975).
19. Materials and methods are available as supplementary materials on *Science* Online.
20. P. A. McCrory, J. L. Blair, F. Waldhauser, D. H. Oppenheimer, *J. Geophys. Res. Solid Earth* **117**, n/a (2012).
21. W. P. Schellart, J. Freeman, D. R. Stegman, L. Moresi, D. May, *Nature* **446**, 308–311 (2007).
22. A. F. Holt, B. A. Buffett, T. W. Becker, *Geophys. Res. Lett.* **42**, 3802–3810 (2015).
23. W. Schellart, *J. Geophys. Res. Solid Earth* **115**, B11406 (2010).
24. T. Lay, H. Kanamori, L. Ruff, *Earthq. Predict. Res.* **1**, 3 (1982).
25. S. T. Tse, J. R. Rice, *J. Geophys. Res.* **91**, 9452 (1986).
26. J. Dieterich, *J. Geophys. Res. Solid Earth* **99**, 2601–2618 (1994).
27. C. H. Scholz, *Nature* **391**, 37–42 (1998).
28. C. Marone, *Nature* **391**, 69–72 (1998).
29. Y. Guglielmi, F. Cappa, J.-P. Avouac, P. Henry, D. Elsworth, *Science* **348**, 1224–1226 (2015).
30. B. P. Allmann, P. M. Shearer, *J. Geophys. Res. Solid Earth* **114**, B01310 (2009).
31. K. Wang, S. L. Bilek, *Tectonophysics* **610**, 1–24 (2014).
32. K. Wang, S. L. Bilek, *Geology* **39**, 819–822 (2011).
33. Q. Bletery, A. Sladen, J. Jiang, M. Simons, *J. Geophys. Res. Solid Earth* **121**, 5116–5135 (2016).
34. R. McCaffrey, *Geology* **36**, 263 (2008).
35. K. Satake, K. Wang, B. F. Atwater, *J. Geophys. Res. Solid Earth* **108**, 2535 (2003).
36. T. Furumura, K. Imai, T. Maeda, *J. Geophys. Res. Solid Earth* **116**, B02308 (2011).
37. F. Dahlen, *Annu. Rev. Earth Planet. Sci.* **18**, 55–99 (1990).
38. R. J. Lisle, J. M. Robinson, *J. Struct. Geol.* **17**, 739–750 (1995).
39. C. R. Ranero, J. Phipps Morgan, K. McIntosh, C. Reichert, *Nature* **425**, 367–373 (2003).
40. M. Faccenda, T. V. Gerya, L. Burlini, *Nat. Geosci.* **2**, 790–793 (2009).
41. T. Nishikawa, S. Ide, *Geophys. Res. Lett.* **42**, 7081–7089 (2015).

## CATALYSIS

# Direct and continuous strain control of catalysts with tunable battery electrode materials

Haotian Wang,[1] Shicheng Xu,[2] Charlie Tsai,[3,4] Yuzhang Li,[5] Chong Liu,[5] Jie Zhao,[5] Yayuan Liu,[5] Hongyuan Yuan,[6] Frank Abild-Pedersen,[4] Fritz B. Prinz,[2,5] Jens K. Nørskov,[3,4] Yi Cui[5,7]*

We report a method for using battery electrode materials to directly and continuously control the lattice strain of platinum (Pt) catalyst and thus tune its catalytic activity for the oxygen reduction reaction (ORR). Whereas the common approach of using metal overlayers introduces ligand effects in addition to strain, by electrochemically switching between the charging and discharging status of battery electrodes the change in volume can be precisely controlled to induce either compressive or tensile strain on supported catalysts. Lattice compression and tension induced by the lithium cobalt oxide substrate of ~5% were directly observed in individual Pt nanoparticles with aberration-corrected transmission electron microscopy. We observed 90% enhancement or 40% suppression in Pt ORR activity under compression or tension, respectively, which is consistent with theoretical predictions.

**H**ighly efficient electrocatalysts for renewable energy conversion processes, such as in $H_2$ fuel cells and water-splitting electrocatalysis, is becoming increasingly important (*1–3*). One strategy for systematically improving the activities of known catalysts is to modify their electronic structure (*4–6*). Numerous examples have been demonstrated in $H_2O$–$O_2$–$H_2$ electrocatalysis, such as the changing of d band filling in perovskite oxides for oxygen evolution (*7*), transition-metal alloying for the oxygen reduction reaction (ORR) (*4, 8–11*), and our recent studies of using lithium (Li)–ion intercalation and extraction in layered materials for water-splitting (*12, 13*).

Lattice strain, either compressive or tensile, can alter the surface electronic structure by mod-ifying the distances between surface atoms and in turn catalytic activity (*14–17*). For platinum (Pt), previous studies have suggested that the 5d-band center of Pt can be shifted by ~0.1 eV with only 1% lattice strain (*18*), which can appreciably strengthen or weaken bonding of reaction intermediates to the surface (*14, 18*). Lattice-mismatch between metals can be generated by directly synthesizing core-shell structures (*19–23*) or by selectively removing atoms from an alloy (for example, stripping away Cu from a Pt-Cu alloy) (*8, 14, 24–26*). However, because of the larger lattice of Pt as compared with that of most metal cores, this method is typically restricted to compressive strain (*14, 27*). Additionally, both electronic charge transfer between the different metal atoms (ligand effects) and changes in the surface stability—and thus surface area—are present, making it difficult to identify and control the effects of strain alone (*14, 25*). Another strategy is to deposit catalysts onto flat substrates that undergo physical transformations as external forces are applied or the temperatures varied (*28, 29*). Those flat and tunable substrates present great importance to fundamental analysis, but only a few of them have been successfully demonstrated effective in electrocatalysis (*28*). Thus, new methods that can flexibly and effectively control both tensile and compressive lattice strain in catalysts without introducing additional effects are needed.

[1]Department of Applied Physics, Stanford University, Stanford, CA 93205, USA. [2]Department of Mechanical Engineering, Stanford University, Stanford, CA 93205, USA. [3]SUNCAT Center for Interface Science and Catalysis, Department of Chemical Engineering, Stanford University, Stanford, CA 94305, USA. [4]SUNCAT Center for Interface Science and Catalysis, SLAC National Accelerator Laboratory, 2575 Sand Hill Road, Menlo Park, CA 94025, USA. [5]Department of Material Science and Engineering, Stanford University, Stanford, CA 94305, USA. [6]Department of Physics, Stanford University, Stanford, CA 94305, USA. [7]Stanford Institute for Materials and Energy Sciences, SLAC National Accelerator Laboratory, 2575 Sand Hill Road, Menlo Park, CA 94025, USA.
*Corresponding author. Email: yicui@stanford.edu

Editor's Summary

### Mega-earthquakes go the flat way

Megathrust faults in subduction zones cause large and damaging earthquakes. Bletery *et al.* argue that certain geometric features of the subduction zones relate to earthquake size. The key parameter is the curvature of the megathrust. Larger earthquakes occur where the subducting slab is flatter, providing a rough metric for estimating where mega-earthquakes may occur in the future.

*Science*, this issue p. 1027

| | |
|---|---|
| **Article Tools** | Visit the online version of this article to access the personalization and article tools:<br>http://science.sciencemag.org/content/354/6315/1027 |
| **Permissions** | Obtain information about reproducing this article:<br>http://www.sciencemag.org/about/permissions.dtl |